IBIS 2.0

Science Description

Document number: IBIS-02

Document version: 5

Released on: 2021-05-01

Prepared by: Paolo Romano

Authors

Name	Affiliation
Dario Del Moro	UNIToV
Salvatore Luigi Guglielmino	UNICt / INAF - OACt
Mariarita Murabito	INAF – OAR
Paolo Romano	INAF - OACt

Change record from previous version

Affected section(s)	Changes / Reason / Remarks
All	Updates after review for submission to INAF Open Access repository.

Contents

1 Introduction

1.1 Purpose

The Interferometric BIdimensional Spectrometer 2.0 (IBIS 2.0) is a focal plane instrument which will be developed to acquire high cadence spectroscopic and spectropolarimetric images of the solar photosphere and chromosphere. Its previous version, named IBIS, was installed at the focal plane of the Dunn Solar Telescope of the National Solar Observatory in New Mexico (USA). It used two FPI in a classic mount and operated over the range 580 – 860 nm. IBIS 2.0 provides an important opportunity to investigate many open questions regarding the physics of the solar atmosphere, with particular attention to the phenomena visible in the photosphere and chromosphere. Moreover, IBIS 2.0 could represent a first step to develop a new instrument for the next generation telescopes. A brief overview of the project is available in [RD4].

A Science Working Group (SWG) has been charged by the project with the task of identifying the key science goals for the new version of the instrument and defining the corresponding science requirements that are needed to accomplish those goals. This document reports the outcome of such a Science Working Group.

1.2 Scope

This document contains the most important science objectives where IBIS 2.0 can provide a significant contribution to their understanding. The scope of this document is to provide the science requirements necessary to tackle high-level science questions involving the coupling between the plasma and the magnetic field in the solar atmosphere. For this reason, we described some science cases and open questions from which to derive the technical requirements for the instrument development. We focused on some specific examples that can be investigated by the contribution of IBIS 2.0 data in the visible range and we also provided the useful parameters for the execution of some observing programs suitable for the study of the reported science cases. We highlighted the importance of the synergy between IBIS 2.0 and the other ground-based instruments for high-resolution observations of the lower layers of the solar atmosphere, as well as with satellite observations. Finally, we summarized the main useful scientific information for the instrument development.

1.3 Definitions, acronyms and abbreviations

ALMA	Atacama Large Millimeter Array
CME	Coronal Mass Ejection
CP	Circular Polarization
CHROMIS	CHROMospheric Imaging Spectrometer
CRISP	CRisp Imaging SpectroPolarimeter
Cryo - NIRSP	Cryogenic Near Infra-Red Spectro-Polarimeter
DKIST	Daniel K. Inouye Solar Telescope
DST	Dunn Solar Telescope
EF	Evershed flow
EFR	Emerging Flux Region

EST	European Solar Telescope
FPI	Fabry-Perot Interferometer
GFPI	GREGOR Fabry-Perot Interferometer
GRIS	GREGOR Infrared Spectrograph
GST	Goode Solar Telescope
HAO	High Altitude Observatory
IBIS	Interferometric BIdimensional Spectrometer
IBIS 2.0	Interferometric BIdimensional Spectrometer 2.0
INAF	Istituto Nazionale di Astrofisica
LARS	Laser Absolute Reference Spectrograph
LB	Light Bridge
MHD	Magnetohydrodynamic
MMFs	Moving Magnetic Features
NIR	Near Infrared
NIRIS	Near Infrared Imaging Spectropolarimeter
NIRSP	Near-IR Spectro-polarimeter
NSO	National Solar Observatory
NUV	Near Ultraviolet
OACT	Osservatorio Astrofisico di Catania
OAR	Osservatorio Astronomico di Roma
PIL	Polarity Inversion Line
RBEs	Rapid Blueshifted Excursions
Ra	Rayleigh number
ROSA	Rapid Oscillations in the Solar Atmosphere
SST	Swedish Solar Telescope
SWG	Science Working Group
TESOS	Triple Etalon SOlar Spectrometer
THEMIS	Téléscope Héliographique pour l'Etude du Magnetisme et des Instabilité Solaires

UD	Umbral Dot
UNICT	Università degli Studi di Catania
UNIToV	Università di Roma “Tor Vergata”
UP	Umbra-Penumbra
VIS	Visible Imaging Spectrometer
VISP	Visible Spectro-Polarimeter
VTT	Vacuum Tower Telescope
WLF	White Light Flare

2 Related Documents

RD1 IBIS2.0 - Operation and Calibration Plan (IBIS-03)

RD2 IBIS2.0 - IBIS at DST: Optomechanical Layout and Instrument Control (IBIS-05)

RD3 Exploiting Observations at NUV and NIR Wavelengths: Research Goals and Costs (IBIS-06)

RD4 IBIS 2.0 Project Status - Executive Summary (IBIS-PSR-01)

3 Science goals for IBIS 2.0

The main goal of IBIS 2.0 is to provide high spatial and temporal spectropolarimetric data to the scientific community in order to answer many open questions of Solar Physics. Using data taken in the visible range between 580 nm and 860 nm, IBIS 2.0 will allow investigating several issues related to the plasma dynamics and magnetic field properties at photospheric and chromospheric levels.

For the IBIS instrument a set of twelve prefilters was available. The relevant lines that could be observed through these prefilters are reported in Table 1.

Fe I 543.4 nm (g=0) h^{6}= 550 km	He I D3 587.6 nm h^{8}= 1100-1800 km	Na I D2 589.0 nm h^{10}= 600 km	Na I D1 589.6 nm (g=1.33) $h^{4,9}$ = 800-1000 km	Fe I 617.3 nm (g=2.5) h^{7}= 250-350 km	Fe I 630.1 nm / 630.2 nm (g=1.67/2.5) $h^{6}_{630.1}$= 340 km $h^{6}_{630.2}$= 250 km
H I (Hα) 656.3 nm h^{11}= 1500 km	Ni I 676.8 nm (g=1.43) h^{1}= 200 km	Fe I 709.0 nm (g=0) h^{3}= 100 km	Fe II 722.4 nm (g=0) h^{3}= 50 km	K I 769.9 nm h^{5}= 400 km	Ca II 854.2 nm (g=1.10) h^{2}= 200-1300 km

Table 1: List of prefilters of the IBIS instrument. For each prefilter, the corresponding ion, its wavelength, Landé factor and formation height have been reported. The superscript numbers indicate the corresponding references listed for Section 3, reported in Section 6.

However, we will focus our analysis of the scientific requirements on a subset of lines, including the most used ones in spectropolarimetry of the photosphere and chromosphere: e.g., Fe I 617.3 nm (same as SDO/HMI and SolO/PHI), Fe I 630.1 nm and 603.2 nm (same as Hinode/SP), Ca II 854.2 nm (also used by CRISP) lines as representative lines, also for the ease of comparison with other instruments. Using such an approach, we aim at providing a first benchmark for the implementation of IBIS 2.0. All the same, we do not intend to curb the potentiality of the instrument: clearly, other lines included in the set of prefilters may be used for the scientific exploitation. Conversely, we foster development of the instrument to include other useful lines in the visible that were not used in the previous version, such as the Fe I 557.6 nm line. Similarly, other science cases can be designed and exploited using different observational setups.

In the following, we will describe some among the main open scientific questions that can be addressed by IBIS 2.0. For each scientific case, we will provide tables with the corresponding scientific requirements for the instrumental setup, also indicating some representative sets of useful lines. The standard samplings for each spectral line are reported in the Appendix A of [RD1]. When polarimetry is needed, a minimum polarimetric sensitivity of 10^{-3} times the continuum intensity level is meant to be required, which corresponds to the former IBIS polarimetric sensitivity (Viticchié et al. 2010).

Note that the values indicated in the tables are intended to be minimum requirements to be met in order to achieve significant progress in the understanding of the relevant physical processes. On the other hand, we point out that many of the open scientific questions could benefit from a significant progress even if the proposed requirements will be fulfilled with some trade-offs.

3.1 Key science for Solar Physics

The solar atmosphere is an extremely dynamic environment, characterized by a continuous interplay between plasma and magnetic field. Such interaction plays a fundamental role in hugely diverse astrophysical systems, but on the Sun it occurs at scales that cannot be studied outside the solar system.

The combination of the results expected from state-of-the-art high-resolution instruments performing multi-wavelength imaging and polarimetry with detailed numerical inversions of the spectropolarimetric data offers the promise to gain understanding of the physical processes in the solar atmosphere that are presently most disputed, because they are either newly recognized or are currently generating substantial debate.

The know-how gained in the recent years on the analysis of high-resolution observations and on numerical techniques applied for investigating the fine structure and dynamics of the Sun needs new instrumental capabilities to better investigate several physical phenomena that occur in the lower layers of the solar atmosphere, affecting indirectly the whole heliosphere.

Many steps of the research in Solar Physics are still necessary for understanding the interplay between the plasma and the magnetic field in generating the heating of the solar atmosphere and driving the evolution of the large-scale solar magnetic structures. Both subjects figure in the ASTRONET Science Vision document for European Astronomy and ESA COSMIC VISION 2015-2025 document.

The coronal heating problem is one of the longest running solar physics puzzles and is still a highly controversial topic. Considerable progress has been made in modelling possible heating mechanisms. However, discriminating among these mechanisms to determine the dominating process has been extremely difficult to achieve. This is because the corona is not energetically isolated from the other regions of the atmosphere, such as the photosphere and chromosphere, rather the whole of the solar atmosphere forms a highly coupled non-linear system, with both energy and mass transferred in both directions between the inner and outer regions. The highly dynamical nature of the solar atmosphere depicted by the most recent high-resolution observations supports the occurrence of complex processes and further motivates the study of their relative contribution to different structures and heights of the solar atmosphere.

The plasma-field interplay in the solar atmosphere is also responsible for the evolution of large-scale magnetic features that are observed to be the source and location of instabilities affecting the space weather. Recent high-resolution observations have shown that sunspots consist of dynamically evolving small-scale and short-living features that all together form coherent large and long-living sunspots and then drive the evolution of magnetic field that permeates the heliosphere.

Nonetheless, despite the recent breakthroughs in solar observations, it is clear that the fundamental scales of the observed processes are still unresolved. Therefore, further high-resolution observations are necessary to provide a useful contribution to solve many debated scientific questions concerning the plasma-field interplay. In this context, IBIS 2.0 can provide a significant contribution, in particular concerning the following key science goals.

3.2 Quiet Sun

The studies on turbulent convection and on the formation, evolution, organization and dissipation of magnetic fields in the quiet Sun may greatly benefit from new data acquired with IBIS 2.0, especially in the case it will be used to construct a database of dedicated observations with a standard acquisition procedure.

3.2.1 Formation, transport and dissipation of small-scale kG flux concentrations

Magneto-convection is a ubiquitous process in the solar surface. The interaction between magnetic fields and the turbulent photospheric convection leads to the formation and evolution of magnetic

features (organized in flux tubes or sheets) and a broad range of flows and waves on various spatial and temporal scales. This makes the photosphere highly dynamic and the place where heating of the upper solar atmosphere could be initiated via small-scale flux emergence, flux cancellation, braiding of magnetic field lines, or generation and upward propagation of waves. All these processes feed the upper atmosphere of energy and are able to trigger a chain of phenomena which are also relevant for the Space Weather.

The magnetic field of these flux tubes is as strong as 1500 G (e.g., Bellot Rubio et al. 2000; Utz et al. 2013), i.e., well above the equipartition value of a few hundred G. Therefore, in addition to the kinematic concentration of flux by horizontal convective motions, another mechanism capable of enhancing the field up to kG strengths is required. In the late 1970s, it was theoretically proposed that the field is amplified by a thermal instability known as convective collapse (Parker 1978; Spruit 1979). This process leads to rapid downflows in the tube's interior, causing a strong evacuation of the magnetic element and a concentration of the field. The spatial and temporal scales associated with the formation of intense flux tubes are on the order of 100 km (corresponding to about 0.14″) and 30 s, according to numerical simulations by Danilovic et al. (2010). These processes deserve to be studied at their intrinsic spatial and temporal scales, with the further requirement on the polarimetric sensitivity needed to measure them, since the physical processes that lead to the appearance and disappearance of kG flux tubes are still not well understood. The evolution and eventual disappearance of flux tubes would be a natural consequence of their interaction with convective motions if they are a surface phenomenon, as indicated by recent numerical simulations. On the other hand, the persistence of some network features suggests that they are rooted below the solar surface. In that case, other mechanisms might be responsible for the disappearance of the flux. What we observe is that while small-scale magnetic elements change shape, move around being pushed by the photospheric convection, and interact with other flux concentrations, merging or cancelling with them (Viticchié et al. 2009, 2010; see Figure 1), on the large scales, network regions do not change significantly in the course of hours/days.

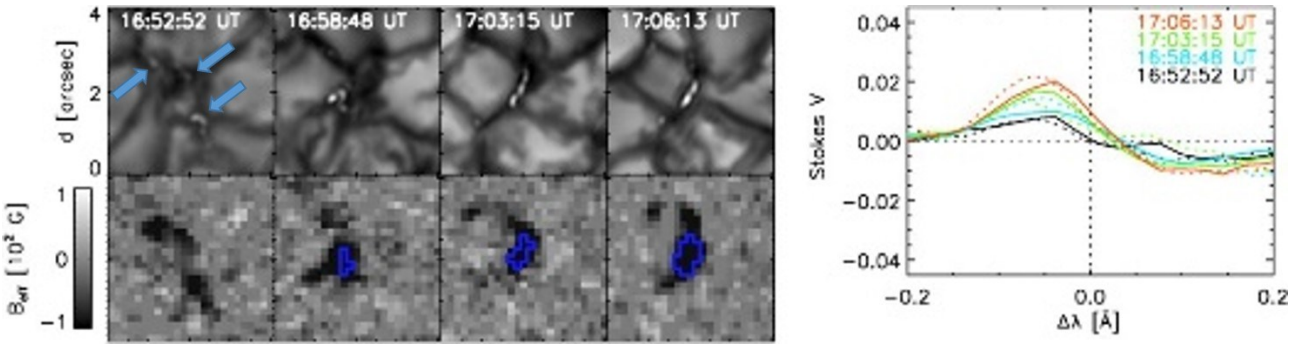

Figure 1: (Adapted from Viticchié et al. 2009). Selection of four instants from the coalescence process of bright points, as observed by IBIS. First row: G-band filtergrams. The arrows indicate the magnetic elements merging and forming the bright point. Second row: center-of-gravity magnetic flux density (images are saturated at ±100 G). Contour plot: kG fields regions as obtained from the inversion analysis of Stokes V profiles. Right plot: Fe I 630.15 nm (dotted line) and Fe I 630.25 nm (solid line) Stokes V profiles calculated as an average over a 0.5″x0.5″ box around the position of the strongest magnetic flux densities for each instant.

3.2.2 Turbulent solar convection

Many aspects of turbulent convection are still far to be completely unveiled. One reason is that the typical Rayleigh number (Ra) expected for solar convection is several orders of magnitude higher than those currently attainable in laboratory experiments (Ra ~10^{17}), so that it is still impossible to test on Earth any theory explaining the onset of turbulent convection in the solar photosphere (see, e.g., Hanasoge et al. 2012). The solar photosphere still represents an unequalled natural laboratory to investigate the nature and the physics of turbulent convection with high Rayleigh number (e.g., Berrilli et al. 2005) and in the past years, IBIS and similar instrumentation have been used to get insights on photospheric turbulent convection with two different approaches:

- *The statistical analysis of plasma and/or magnetic features appearing in the photosphere on several spatial and temporal scales* (e.g., Giannattasio et al. 2018). The analysis of long-time duration data provided constraints on the appearance and evolution of these features via the correlation of coherent photospheric patterns in the quiet Sun, but it gave no many details on the dynamic processes and laws at work.
- *The study of advection/diffusion processes in the photosphere by tracking of magnetic elements in magnetograms or bright features in G-band images* (e.g., Giannattasio et al. 2013, 2014a,b; Del Moro et al. 2015; Abramenko 2017, 2018) under the reasonable hypothesis that these magnetic elements in the quiet Sun are passively transported by the plasma flow (Petrovay & Szakaly 1993; Giannattasio et al. 2013).

In the context of the investigations relevant to the quiet Sun magnetism, IBIS 2.0 will be able to deal with the following main open questions:

- **Are the small-scale kG flux concentrations related with the global dynamo?**
- **What are the physical processes behind flux decay?**
- **Which contribution is provided by small-scale flux concentrations to solar irradiance along the cycle?**
- **What are the properties of the turbulent convection?**

IBIS 2.0 will enhance our information these questions by providing:

1) patrol observations at disc center;
2) photospheric Doppler velocities and horizontal motions at different heights;
3) magnetic fluxes of the quiet Sun patches and their spectropolarimetric characterization;
4) observations of any counterpart in the upper atmospheric layers, up to the chromosphere.

In the following Table 2 and Table 3, we suggest possible observing modes for patrol observations and quiet Sun dynamics, respectively.

	FOV and minimum spatial resolution	**S/N ratio**	**Wavelength**	**Observing mode (N° of spectral points, step for each spectral line)**	**Purpose**	**Minimum cadence and duration of observing run**
Phot.	40″ x 80″ @0.2″	500	Broad-Band	1 image for each spectral point	Horizontal motion Photospheric magnetic field and Doppler measurements Doppler measurements at two photospheric heights	60 s 1.5 hours per day
			Fe I 617.3	25 pt. step 4 pm, pol		
			Fe I 557.6 Fe I 543.4	20 pt. step 4 pm, no pol (each line)		

Table 2: Patrol observations.

	FOV and minimum spatial resolution	S/N ratio	Wavelength	Observing mode (N° of spectral points, step for each spectral line)	Purpose	Minimum cadence and duration of observing run
Phot.	40″ x 40″ @0.2″	500	Broad-Band	1 image for each spectral point	Horizontal motions	75 s 2 hours of good seeing
			Red continuum 668.4	1 pt	Magnetic field diagnostic and Doppler measurements	
			Fe I 630.2	20 pt, step 5 pm, pol (630.15 & 630.25) 15 pt, step 4 pm, pol (630.15 only)		
Chrom.	40″ x 40″ @0.2″	300	Hα 656.28	10 pt, step 6 pm, no pol	Response of the low and mid chromosphere	
			Ca II 854.2	15 pt, step 6 pm, pol		

Table 3: Quiet Sun dynamics.

3.3 Magnetic structure of sunspots

High-resolution spectropolarimetric images of the photosphere and chromosphere allow studying several fine structures of the sunspots and to understand the physical mechanisms that characterize their formation and evolution.

A first scientific interest for IBIS 2.0 deals with the subsurface structure of the sunspots, i.e., whether the magnetic field is clustering or monolithic (Solanki 2003). To solve this problem, it is useful the study of **umbral dots** (UDs), which are transient intensity enhancements observed in sunspot umbrae and pores, with a typical scale of 300 km diameter and 10 min lifetime (e.g., Louis et al. 2012). UDs are considered to be a natural consequence of the interaction between the convection and the magnetic field (Bharti et al. 2010). Their origin is still unclear. Simulations of magnetoconvection performed by Rempel (2012) show that convective motions inside the umbra push out the boundary of the magnetic field lines inside the convective cell, creating a region of strongly reduced field strength, and forming a cusp or canopy field configuration. However, a clear interpretation of the subsurface structure of the sunspots could be given by observations of magnetic field vector and Doppler velocities in and around UDs with spatial resolution around 0.1″. There are many open questions associated with UDs. Are they heated due to oscillatory magnetoconvection, penetration of hot plasma between thin flux tubes or electric currents? Why do UDs move horizontally? Are there chromospheric counterparts of UDs? To provide an answer to these questions, IBIS 2.0 must acquire time series of high spatial resolution magnetic and Doppler maps with temporal resolution of about 60 s, sequentially in the photosphere and chromosphere.

Moreover, we need many photons to reach enough signal-to-noise ratio in the umbra, where the brightness is typically 10% of the brightness in the quiet photosphere.

Mature sunspots are usually surrounded by regions of radially outward **moving magnetic features** (MMFs, Hagenaar & Shine 2005). The origin of these so-called sunspot moats is not well understood. MMFs appear as either unipolar magnetic features or bipolar feature pairs. The unipolar MMFs can have either the same or opposite polarity with respect to the parent spot (Shine & Title 2001). Their typical size is below 2″ and they exhibit a broad range of horizontal velocity from 0.1 to 1.5 km s^{-1} (Harvey & Harvey 1973). A study by Criscuoli et al. (2012), using data from IBIS at NSO/DST, investigating 6 unipolar MMFs around a pore, out of which 3 were of opposite polarity to the pore, confirmed that opposite-polarity MMFs move faster than same-polarity MMFs (see Figure 2).

Recently, it has been suggested that the MMFs are extensions of penumbral filaments which turn back below the visible solar surface at the sunspot magnetopauses and reappear as MMFs in the moats. Indeed, observations by Sainz Dalda & Bellot Rubio (2008) support this so-called sea-serpent model (Schlichenmaier 2002). On other hand, latest studies have confirmed that MMFs can be also observed around sunspots without a penumbra, i.e., around pores (Zuccarello et al. 2009; Verma et al. 2012), showing that a penumbra is not essential for the presence of MMFs.

Therefore, despite the existing studies on MMFs, it is not yet clear to what extent the origin of MMFs is related to the presence of a penumbra or not. Furthermore, these features have to be investigated by IBIS 2.0 in order to shed light on the physical mechanisms which are able to transport the magnetic field from the sunspots to the surrounding network and allow the decay of the sunspots.

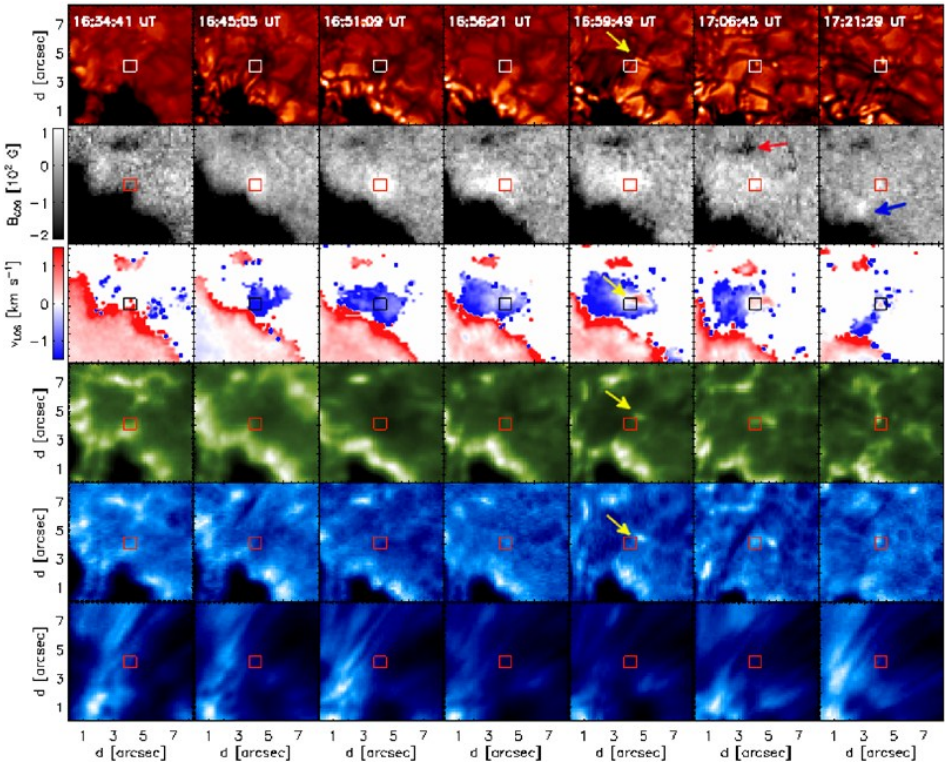

Figure 2: (Adapted from Criscuoli et al. 2012). Representative 8″×8″ frames extracted from the complete temporal evolution of a MMF. From the top to the bottom: G-band filtergrams; LOS magnetograms (clipped at +100 and −200 G) derived with center-of-gravity method; LOS velocity fields as derived from the Stokes V zero-crossing point (clipped at ± 1.5 km s^{-1}); Fe I core images; Ca II wing images; Ca II core images. The red box is centered on the maximum of the LOS magnetic flux within the structure. Yellow arrows in the fifth column mark the formation of bright features in filtergrams and G-band frames and the corresponding formation of a downflow within the MMF. The red arrow on the magnetogram of the sixth column marks a small magnetic region of opposite polarity with respect to the MMF. The blue arrow on the LOS magnetogram of the last column marks another MMF.

Light bridges (hereafter LBs) are elongated bright structures separating the dark umbra of sunspots into two or more magnetically similar polarity regions. It is unclear whether LBs are indeed field-free intrusions of plasma protruding from deep within the photosphere (Spruit and Scharmer 2006) or signatures of magnetoconvection (Rimmele 1997). However, recent observations widely suggest that convective motions of weak-field plasma can penetrate a vertically oriented strong magnetic field from below the photosphere and form a magnetic field canopy configuration near the visible surface.

Dark lanes are seen along the main axes of LBs that look like the high points of ridges in flux tubes (Lites et al. 2004). They are a consequence of the higher density compared with the surrounding environment, which shifts the surface of optical depth unity (tau = 1) toward higher layers, where the temperature is lower in the stratified atmosphere (Spruit & Scharmer 2006; Rimmele 2008).

The LB can also produce chromospheric plasma ejections intermittently and recurrently, seen as surges in Hα (Asai et al. 2001). Shimizu et al. (2009) suggested that these ejections are due to current-carrying highly twisted magnetic flux tubes trapped along the LB below a canopy structure of the umbral fields, forming the magnetic configuration preferable for magnetic reconnections at low altitudes.

Fast downflows with velocities up to 10 km s^{-1}, which is supersonic at the photosphere, have also been observed. Louis et al. (2009) suggested that the flows were due to magnetic reconnection in the upper photosphere/lower chromosphere, although other mechanisms could not be ruled out.

Another interesting structure of the sunspots is the penumbra, whose properties and evolution require particular attention for many aspects which are still not completely understood. Open questions concerning the penumbra are described in the following section.

With regard to the magnetic properties of sunspots and their fine structures, IBIS2.0 will allow us to investigate the following scientific questions:

- **Are there chromospheric counterparts of *umbral dots*?**
- **Are *umbral dots* heated due to oscillatory magnetoconvection, penetration of hot plasma between thin flux tubes or electric currents?**
- **Are *moving magnetic features* extensions of penumbral filaments?**
- **Which is the source of *plasma jets in sunspot light bridges*?**

In particular, IBIS 2.0 will enable us to study:

1) the intensity variations, related to different heating mechanisms;
2) the spectropolarimetric characteristics of sunspot fine structure at different heights;
3) photospheric plasma motions, via Doppler measurements and tracking of the horizontal motions of sub-structures;
4) the magnetic fluxes of UDs, MMFs and LBs along with their spectropolarimetric signatures, both in the photosphere and in the chromosphere.

In the following Table 4, Table 5 and Table 6, we suggest possible observing modes for studies relevant to UDs, MMFs, and LBs, respectively.

	FOV and minimum spatial resolution	**S/N ratio**	**Wavelength**	**Observing mode (N° of spectral points, step for each spectral line)**	**Purpose**	**Minimum cadence and duration of observing run**
Phot.	40″ x 80″ @0.16″	1000	Broad-Band	1 image for each spectral point	Horizontal tracking of the UDs Magnetic field properties of the UDs Doppler measurements in and around UDs	120 s 2 hours
			Fe I 617.3	20 pt. step 4 pm, pol		
			Fe I 630.15 & 630.25	30 pt, step 4 pm, pol		
Chrom.	40″ x 80″ @0.16″	500	Hα 656.28	17 pt, step 2 pm, no pol	Identify the chromospheric counterpart of the UDs	
			Ca II 854.2	20 pt, step 6 pm, pol		

Table 4: Umbral Dots.

	FOV and minimum spatial resolution	S/N ratio	Wavelength	Observing mode (N° of spectral points, step for each spectral line)	Purpose	Minimum cadence and duration of observing run
Phot.	40″ x 80″ @0.2″	500	Broad-Band	1 image for each spectral point	Horizontal tracking of the MMFs Magnetic field properties of the MMFs Measurements of magnetic field cancellation	120 s 2 hours
			Fe I 617.3	20 pt. step 4 pm, pol		
			Fe I 630.15 & 630.25	30 pt, step 4 pm, pol		
Chrom.	40″ x 80″ @0.2″	500	Hα 656.28	17 pt, step 2 pm, no pol	Chromospheric configuration of the sunspot	
			Ca II 854.2	20 pt, step 6 pm, pol		

Table 5: Moving Magnetic Features.

	FOV and minimum spatial resolution	**S/N ratio**	**Wavelength**	**Observing mode (N° of spectral points, step for each spectral line)**	**Purpose**	**Minimum cadence and duration of observing run**
Phot.	40″ x 80″ @0.16″	500	Broad-Band	1 image for each spectral point	Geometrical properties of the LB granules Magnetic field properties of the LB dark lane Doppler measurements of LB jets	120 s 4 hours
			Fe I 617.3	20 pt. step 4 pm, pol		
			Fe I 630.15 & 630.25	30 pt, step 4 pm, pol		
Chrom.	40″ x 80″ @0.16″	300	Hα 656.28	17 pt, step 2 pm, no pol	Doppler measurements of LB jets Identification of chromospheric brightenings near LB jets	
			Ca II 854.2	20 pt, step 6 pm, pol		

Table 6: Light Bridges.

3.4 Penumbra formation, evolution and decay

In the context of sunspot investigation, the formation, evolution and finally the decay of a penumbra is one of the least observed physical processes. In fact, its study requires long time series observations with high temporal, spatial and spectral resolution, which are difficult to achieve.

These phases in the evolution of a sunspot are useful to describe the plasma-magnetic field interplay and the conditions needed for unstable and stable penumbral filaments. Concerning the penumbra formation, two are the scenarios proposed to explain the existing observations. The first suggests that emerging, horizontal field lines could be trapped and form a penumbra rather than continuing to rise to higher layers, due to the presence of an overlying magnetic canopy (Leka & Skumanich 1988). The second arises from observations of the chromospheric structure overlying sunspot with forming penumbrae, which reveal an annular zone around pores earlier than the photospheric penumbral filaments (Shimizu et al 2012; Romano et al 2013, 2014). In the latter, the idea is that the magnetic field, already existing at higher level of the solar atmosphere and overlying the pore, sinks down into the photosphere changing its inclination. From the few existing observations, some authors assessed the presence of critical values for the involved physical parameters above which the penumbra formation takes place. In this regard, a threshold of 1-1.5 x 10^{20} Mx in the magnetic flux has been estimated in order a pore can develop a penumbra (Leka & Skumanich 1988). Furthermore, Jurčák et al. (2011) proposed a critical value of the vertical component of the magnetic field (B_{ver}) at the umbra-penumbra (UP) boundary for mature sunspots. In particular, during the penumbra formation process, Jurčák et al. (2015) found that the UP boundary migrates towards the umbra and B_{ver} increases. The authors proposed two modes of magneto-convection to explain the critical value of B_{ver}.

The penumbra has a typical velocity pattern, the so-called Evershed flow (EF), consisting in a radial outflow along the penumbral filaments themselves. During the early stage of the penumbra formation, it has been reported an opposite flow with respect to the classical EF at some azimuths around pores, which has been considered as a precursor of the former process (Murabito et al. 2016, 2018). The transition between this opposite flow into the classical one needs several hours, and it happens only when the sinking magnetic field dips below the solar surface (see Figure 3).

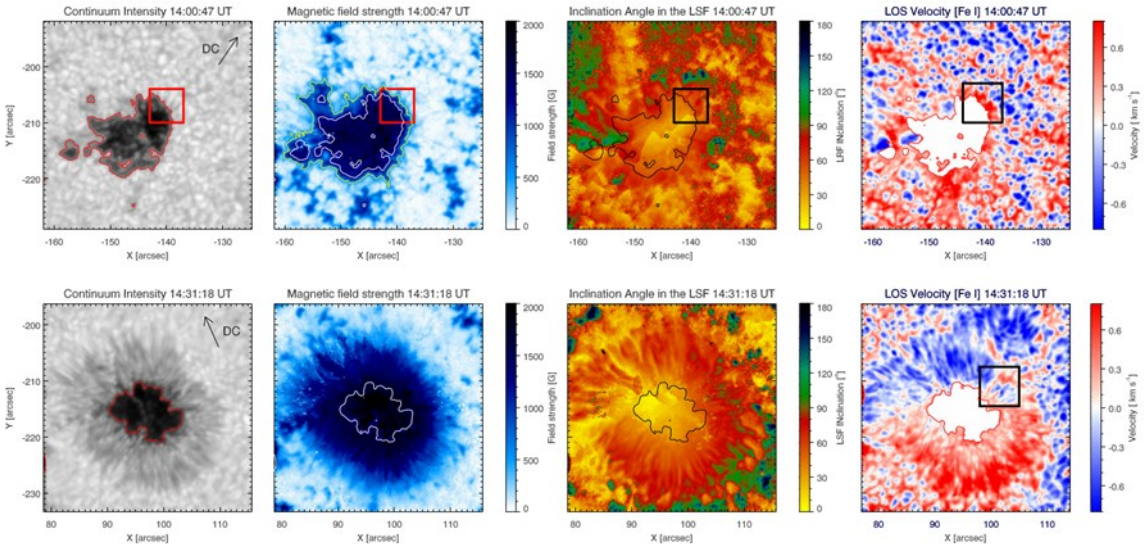

Figure 3: (Adapted from Murabito et al. 2016). Maps of intensity, magnetic field strength, and inclination angle (first, second, and third column) on 2012 May 28 at 14:00 UT (top, before penumbra formation) and on 2012 May 29 at 14:31 UT (bottom, after penumbra formation), obtained from the SIR inversion of the Stokes profiles of the Fe I 630.25 nm line acquired by IBIS. The red or black contours indicate the edge of the pore and of the umbra as seen in the continuum intensity image. In the top panel of the second column, the contours indicate the edge of the pore as seen in the continuum intensity image (red contour) and the annular zone as seen in the magnetic field image (yellow contour), respectively. LOS velocity maps (fourth column) are deduced from the Doppler shift of the centroid of the Fe I 630.25 nm line profile. Downflow and upflow correspond to positive and negative velocities, respectively. The red or black square encloses a region where the transition from inverse to classical Evershed flow during penumbra formation is clearly visible.

In a stable and mature sunspot (e.g., Murabito et al. 2019, 2020), the penumbral filaments consist of a bright head, a dark core along the central axis, and a tail, the difference in the temperature from the heads and the tails reaching up to 800 K (Tiwari et al. 2013). The field topology of the filaments is similar to an inverse U shape, where the field is stronger and vertical (10° - 40°) in the heads, horizontal and weaker in the middle part, then finally stronger and directed downward (140° - 170°) in the tails (for a positive polarity sunspot). The spines (more vertical and stronger field) of the penumbral filaments can be involved in chromospheric brightening events with lifetime less than a minute that heat the transition region, the so-called penumbral microjets (Katsukawa et al. 2007; Bharti et al. 2013). The formation of penumbral microjets seems to be associated with magnetic reconnection between the spine field and the opposite polarity field in the side of filaments (Tiwari et al. 2016).

The decay phase of a sunspot starts with the decrease in size of the penumbral filaments. This process is relatively slow, unless when it is related to solar flares (e.g., Zuccarello et al. 2020), and it remains still poorly understood as the penumbral formation is. The existing observations of penumbral decay (Watanabe et al. 2014; Verma et al. 2018) suggest that the mechanism seems to be exactly the inverse to the above-mentioned formation. In particular, the decay process appears to be due to the rise of photospheric magnetic field lines into the chromosphere. Various aspects about the penumbral decay were extensively investigated, as for example the decay rates or the relation with MMFs. Recently, Benko et al. (2018) studying the evolution of the photospheric magnetic field in a decaying sunspot, found that the Jurčák criterion is no longer fulfilled at the UP boundary.

Up to now, the main question we have to address concerns the role of the magnetic flux emergence and the interaction with the overlying magnetic canopy. In this regard, IBIS 2.0 will be able to shed light on some aspects of these processes. **In particular, the possibility of IBIS 2.0 to acquire spectra consecutively along photospheric and chromospheric spectral lines is fundamental to understand the role of the overlying magnetic canopy for both the penumbra formation and decay processes.**

Thanks to the spectropolarimetric observations of IBIS 2.0, we will investigate the following main open questions:

- **Is the overlying magnetic canopy responsible for both the *penumbra formation and decay* processes?**
- **Is the Jurčák criterion universally valid?**
- **What are the properties of the penumbra as observed in the chromosphere, and how are they correlated with the photospheric dynamics?**

In fact, IBIS 2.0 will provide information about:

1) plasma motions along the penumbral filaments, via Doppler measurements at different heights during penumbra formation and evolution;
2) magnetic field emergence and magnetic topology, both in the photosphere and in the chromosphere, via spectropolarimetry.

In the following Table 7, we suggest a possible observing mode for penumbra evolution.

	FOV and minimum spatial resolution	**S/N ratio**	**Wavelength**	**Observing mode (N° of spectral points, step for each spectral line)**	**Purpose**	**Minimum cadence and duration of observing run**
Phot.	40″ x 80″ @0.16″	500	Broad-Band	1 image for each spectral point	Magnetic field diagnostics	120 s 4 hours
			Fe I 617.3	20 pt. step 4 pm, pol	Velocity diagnostics	
			Fe I 630.15 & 630.25	30 pt, step 4 pm, pol		
Chrom.	40″ x 80″ @0.16″	500	Hα 656.28	17 pt, step 2 pm, no pol	Velocity diagnostics Role of the overlying magnetic canopy	
			Ca II 854.2	20 pt, step 6 pm, pol		

Table 7: Penumbra evolution.

3.5 Magnetic flux cancellation in the low solar atmosphere

The magnetic flux cancellation process is thought to occur at very small scale in the solar atmosphere, providing a possible mechanism for the elusive magnetic field decay (e.g., van Ballegooijen & Martens 1989).

At the photospheric level, magnetic flux patches with opposite polarities can be advected by horizontal motions and come into contact cancelling, partially or totally, with each other, thus removing magnetic flux from the solar atmosphere (Livi et al. 1989). The process is typically accompanied by energy release phenomena, like small jets and brightness enhancements (see Panesar et al. 2016 and references therein), which may be a source of chromospheric and coronal heating. Many layers of the low solar atmosphere, up to the chromosphere, may be involved in flux cancellation.

However, it is still under debate whether cancellation events are due to the interaction between previously unrelated flux systems, triggering magnetic reconnection (Litvinenko 1999), or to dynamical processes involving pre-connected features, such as the submergence of Ω-loops and/or the emergence of U-loops. Indeed, all these mechanisms are likely to contribute to a different extent to the flux removal, so that it is important to determine their relative importance and efficiency. This can be achieved by simultaneous observations of the photosphere and chromosphere, analyzing the plasma flows, the magnetic configuration, and - above all - the timing of the cancelation events observed at different levels of the solar atmosphere.

In this context, Harvey et al. (1999) determined the time difference between the disappearance of quiet-Sun magnetic bipoles from the photosphere and the chromosphere, concluding that magnetic flux is retracting below the surface for most of the cancellation events studied. On the other hand, Chae et al. (2004) observed horizontal fields and enhanced downflows occurring near the polarity inversion line (PIL), supporting the scenario of submerging Ω-loops. Bellot Rubio & Beck (2005) observed two independent, non-collinear flux concentrations approaching each other and cancelling until the smaller one disappeared completely. The cancellation appeared to be due to magnetic reconnection in the photosphere, with a reaction of the chromosphere to changes in the photospheric layers manifesting as enhanced chromospheric emission with a time delay of about 20 minutes.

Another possible way to distinguish between the different mechanisms is offered by spectropolarimetric measurements, which have shown the presence of asymmetric Stokes V profiles along the PIL between opposite polarity patches that undergo reconnection above the photosphere during cancellation events (Kubo et al. 2014; Kaithakkal et al. 2020). Although the lack of spatial resolution may be in part responsible for the observed asymmetry, its evolution seems to be able to provide additional information on the reconnection-related cancellation events.

On the other hand, flux cancellation events have also been correlated to rapid blueshifted excursions (RBEs). These appear to have a common origin with chromospheric type-II spicules, sharing with them some similar properties (e.g., rapid motion and location). This is important in the light of their contribution to coronal heating. Taking advantage of high-cadence imaging spectroscopy along the Ca II 854.2 nm line from IBIS at NSO/DST, Deng et al. (2015) analyzed a sample of RBEs observed in a very quiet region at the disc center (see Figure 4). Investigating the association of RBEs with the concomitant photospheric magnetic field evolution and using coordinated high-resolution and high-sensitivity magnetograms made by Hinode, they were able to find clear examples of RBEs associated to flux cancellation only in about 25% of the events. So, such a correlation should be further investigated.

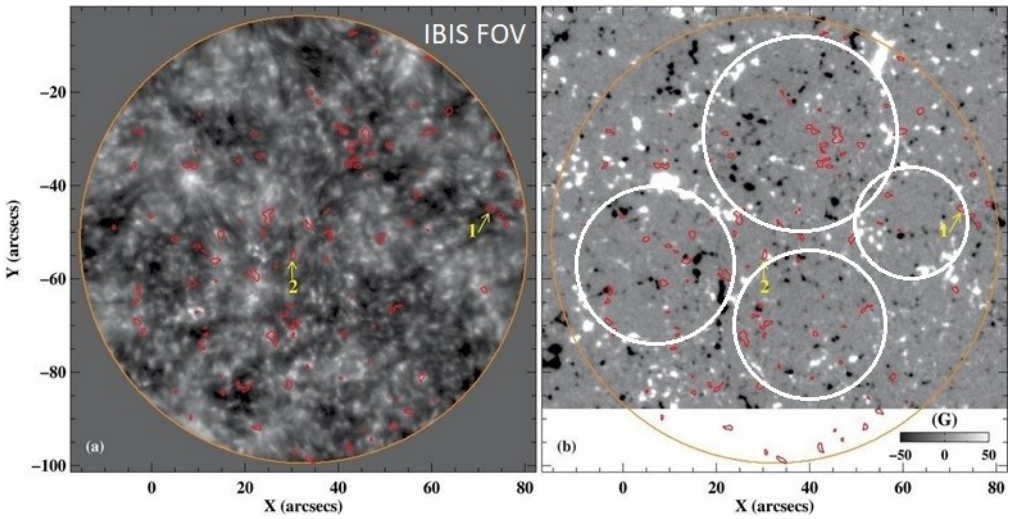

Figure 4: (Adapted from Deng et al. 2015). IBIS Ca II 854.2 nm (a) and Hinode/NFI LOS magnetic field (b) observations of a very quiet region at the disckm center at 16:10 UT on 2011 October 21. The red contours outline the detected 98 RBEs during 16:08:02–16:19:31 UT, 88 of which are in the FOV of Hinode observations (note the magnetogram is scaled from −50 to 50 G). The event 1 and 2, as pointed to by arrows, are a flux emergence and a flux cancellation related event, respectively. The white circles in Panel (b) roughly delineate the supergranular cells. The orange circle indicates the FOV of IBIS.

Overall, the cancellation process remains scarcely studied, since we miss the detection of post-reconnection Ω-loops and U-loops. Only recent observations by the balloon-borne Sunrise mission have addressed the problem again, adding new pieces of information. In fact, Kaithakkal & Solanki (2019) have studied quiet-Sun cancellation events, which result from either field-line submergence, when cancellation happens between a pre-existing large magnetic feature of one polarity and a smaller feature of the other polarity that emerged or appeared nearby (Class I), or reconnection followed by submergence, occurring between two pre-existing previously unconnected features that converge (Class II). Ohmic dissipation of magnetic energy, observed as enhanced emission in the low chromosphere, also seems to play a role for both classes. The dynamics and evolution of these events are strongly influenced by neighboring granular motions. It is worth noting that the flux cancellation rates of the Class II events seem to indicate that they belong to somewhat different category of cancellations when compared with those previously studied with other instruments.

The observations of IBIS 2.0 will provide new insights to study the evolution of flux cancellation events, in order to answer to the following open questions:

- **What is the predominant process of flux cancellation in the low solar atmosphere?**
- **What is the role of magnetic reconnection in flux cancellation? Why does Ohmic dissipation appear not always being at work?**
- **What are the effective flux cancellation rates in the various magnetic environments of the solar atmosphere? Can they represent a source for coronal heating?**

Indeed, IBIS 2.0 will be able to characterize:

1) the horizontal motions that lead to the encounter between opposite polarity patches;
2) the magnetic flux and the magnetic configuration of the cancelling patches;
3) the spectropolarimetric signatures observed in the Stokes profiles emerging from the cancelling patches;
4) the response of the solar atmosphere to the energy release.

In the following Table 8, we suggest a possible observing mode for investigating flux cancellation events.

	FOV and minimum spatial resolution	S/N ratio	Wavelength	Observing mode (N° of spectral points, step for each spectral line)	Purpose	Minimum cadence and duration of observing run
Phot.	20″ x 20″ @0.2″	1000	Broad-Band	1 image for each spectral point	Horizontal motions	90 s 2 hours
			Red continuum 668.4	1 pt	Magnetic field diagnostic	
			Fe I 630.2	20 pt, step 5 pm, pol (630.15 & 630.25) 15 pt, step 4 pm, pol (630.15 only)		
Chrom.	20″ x 20″ @0.2″	500	Hα 656.28	10 pt, step 6 pm no pol	Response of the low and mid chromosphere	
			Ca II 854.2	15 pt, step 4 pm, no pol		

Table 8: Flux cancellation events.

3.6 Interaction between pre-existing and emerging magnetic fields

High-resolution observations show that magnetic flux emergence has a fundamental impact on the evolution of the outer solar atmosphere. Indeed, magnetic interactions between new and pre-existing fields are thought to be crucial for triggering energy release phenomena, from small-scale reconnection episodes to large-scale events such as flares and Coronal Mass Ejections (CMEs).

At the photospheric level, a contact between an emerging magnetic patch and a pre-existing opposite magnetic polarity appears to be the common denominator in many phenomena that are characterized by small-scale transient brightenings and jet-like ejections (Shimizu 2015). In particular, reconnection may occur when an emerging flux region (EFR) interacts with a bundle of pre-existing field lines, in a variety of magnetic environments observed in the solar photosphere (e.g., quiet Sun flux concentrations, plage, MMFs, penumbral filaments). At this point, magnetic reconnection can trigger high-temperature emission in localized regions and surge/jet ejections (Guglielmino 2012; Cheung & Isobe 2014).

Indeed, this scenario has been reported in very detailed high-resolution observations of small-scale EFRs that showed the chromospheric and coronal responses to the photospheric changes induced by flux emergence (Guglielmino et al. 2008, 2010; Vargas Domínguez et al. 2012; Ortiz et al. 2014, 2016; Centeno et al. 2017; Toriumi et al. 2017; Guglielmino et al. 2018, 2019). Numerical radiative

magnetohydrodynamic (MHD) simulations of flux emergence also support this picture, showing that small-scale energy release events occur ubiquitously in the EFRs, as a result of magnetic reconnection. This is found at EFR locations either owing to the interaction of the newly emerged magnetic flux with the pre-existing ambient field or to the self-interaction of the emerging bipolar flux concentrations (e.g., Yokoyama & Shibata 1995; Archontis et al. 2004, 2007; Galsgaard et al. 2007; Cheung & Isobe 2014; Hansteen et al. 2017).

One of the most prominent examples of such bursty energy releases and vigorous heating can be observed in the visible and near-infrared parts of the solar spectrum as small-scale, elongated brightenings sparkling throughout an active region during its emergence. These events are known as 'Ellerman bombs' (Ellerman 1917) and belong to a family of similarly-driven, but height-dependent energy releases during magnetic field evolution, e.g., the so-called UV bursts (Young et al. 2018) and microflares at increasingly higher energy. The ‘Ellerman bomb’ phenomenon is currently a heavily debated subject in both observational (e.g., Nelson et al. 2013; Vissers et al. 2015, 2019; see Figure 5) and numerical studies (Archontis & Wood 2009; Hansteen 2017).

In this respect, it is necessary to carry out the investigation of the evolution of flux emergence episodes and of the interaction between these EFRs and the surrounding atmosphere at several wavelengths, in order to obtain a complete picture of the phenomena taking place at these locations. A multi-layer diagnostics approach allows us to derive some signatures of the rising plasma, e.g., time delays between the passage through different atmospheric heights and vertical velocities through imaging and spectroscopic information, respectively. Furthermore, spectropolarimetric measurements at different heights may reveal the detailed magnetic configuration of both the EFRs and the magnetic environment which they interact with, detailing the connectivities of the emerging magnetic field in the chromosphere. Indeed, the relative orientation of the interacting magnetic fields appears to be the critical parameter that drives the energy release (e.g., Galsgaard et al. 2007).

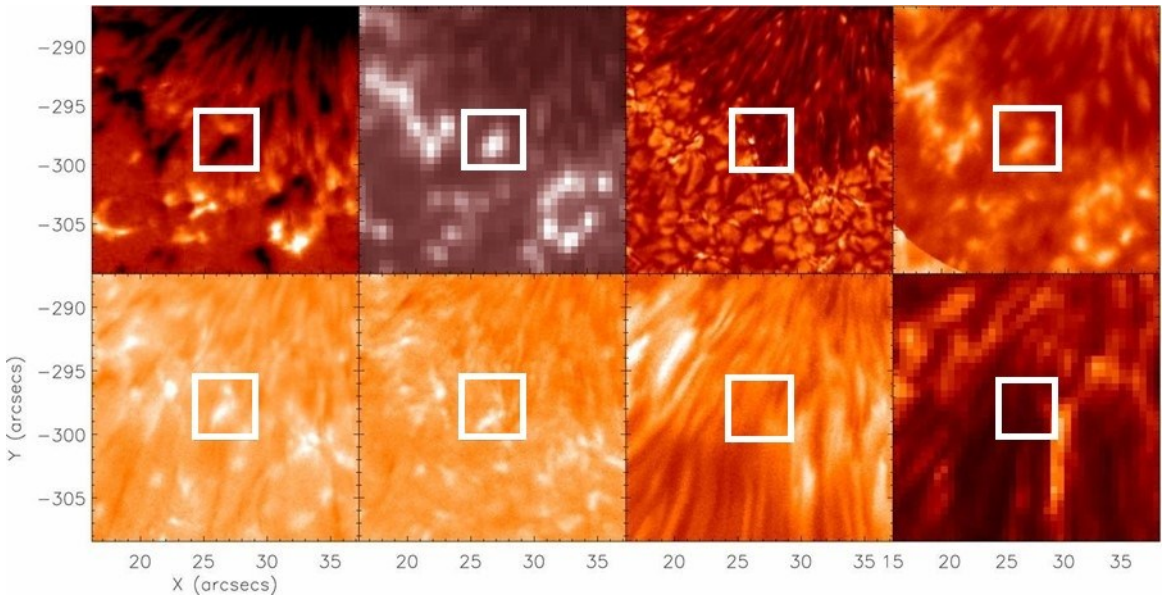

Figure 5: (Adapted from Nelson et al. 2013). Top row (left to right): co-aligned Hinode/SOT Stokes V/I, SDO/AIA 170 nm, ROSA G band, and IBIS Fe I 630.25 nm line core, acquired on 2012 September 30 and relevant to active region NOAA 11579. Bottom row (left to right): IBIS Hα blue and red wing images (approximately ±75 pm), IBIS Hα line core, and SDO/AIA 30.4 nm. The box frames an Ellerman bomb analyzed in detail. This FOV is taken at the temporally closest image for each wavelength to 14:56:35 UT.

In this perspective, IBIS2.0 will be a very suitable facility for studying how the new field reshapes in the local magnetic field as the magnetic regions emerge and evolve, allowing us to address the following open issues:

- **How is the response of the chromosphere with respect to flux emergence related to the pre-existing magnetic environment?**

- **What are characteristic time scales of the response of the various atmospheric layers to flux emergence?**
- **What is the main driver of energy release phenomena during flux emergence?**

Thanks to its polarimetric sensitivity and spectroscopic imaging capabilities, IBIS2.0 will be useful to determine:

1) the magnetic flux and the magnetic configuration of the emerging and pre-existing magnetic patches;
2) the plasma motions observed during the emergence and at the site of interaction, e.g., blue-red spectral enhancements indicating high-speed ejections;
3) the response of the solar chromosphere to the energy release.

In the following Table 9, we suggest a possible observing mode for studying episodes of interaction between emerging and pre-existing flux systems.

	FOV and minimum spatial resolution	**S/N ratio**	**Wavelength**	**Observing mode (N° of spectral points, step for each spectral line)**	**Purpose**	**Minimum cadence and duration of observing run**
Phot.	40″ x 40″ @0.2″	1000	Broad-Band	1 image for each spectral point	Horizontal motions Horizontal motions Magnetic field diagnostic and Doppler measurements	90 s 4 hours
			Red continuum 668.4	1 pt		
			Fe I 630.2	20 pt, step 5 pm, pol (630.15 & 630.25) 15 pt, step 4 pm, pol (630.15 only)		
Chrom.	40″ x 40″ @0.2″	500	Hα 656.28	15 pt, step 6 pm no pol	Response of the mid chromosphere Response of the low chromosphere	
			Ca II 854.2	20 pt, step 4 pm, pol		

Table 9: Interacting flux systems.

3.7 Secondary effects during solar flares

Solar flares are sudden and short-lived release of radiation and particles in the solar atmosphere. The total energy stored and released in the form of flare radiation can be up to 10^{32} erg. This is provided by reconfiguration of non-potential coronal magnetic field to a lower energy state (Priest & Forbes 2000, 2002). Solar flares are often closely associated with CMEs (Harrison 1986), and the most intense radiation is associated with acceleration of non-thermal particles (e.g., Sui et al. 2005). In fact, many flare-CME models are based on the CSHKP (Carmichael 1964; Sturrock 1966; Hirayama 1974; Kopp & Pneuman 1976) magnetic reconnection model. The model requires that a flare occurs just underneath an erupting filament which eventually becomes the core of the CME associated with the flare. Normally the core corresponds to the center of the CME. Flares and CMEs are also the driving features of Space Weather, with significant impact on our technological society.

The centrally important question of flare physics is to understand how the energy stored in stressed coronal magnetic field is released so rapidly, and converted – with very high efficiency – into the kinetic energy of the non-thermal particles and thus, or otherwise, into the flare radiative output (Fletcher & Hudson 2008).

The solar chromosphere remains of primary interest during flares (e.g., Matthews et al. 2003; Metcalf et al. 2003). In fact, it is there that the majority of the flare radiative output originates, making it the main source of flare diagnostic information. Using chromospheric radiation we can deduce flare heating and ionization, and subsequent cooling and de-excitation of different layers of the atmosphere as well as flows, non-thermal velocities, and the character of the non-thermal particle distributions. The energy deposition profile as a function of space and time can in principle be understood by IBIS 2.0 observations of the chromospheric evolution.

IBIS 2.0 will be able to provide a significant contribution to answer to some open questions of the secondary effects visible in the lower layers of the solar atmosphere. What is the energy output of the flaring chromosphere? Is the standard 'collisional thick-target' model for flare energy transport correct? How does the temperature, density and ionization structure of the flare chromosphere respond to time-dependent energy input?

In this context, Kuridze et al. (2016) benefitted from high spectral resolution obtained with IBIS at NSO/DST to study the temporal evolution of the Na I D1 line profiles in the M3.9 flare SOL2014-06-11T21:03 UT (see Figure 6). These profiles show a significant increase in the intensities of the line core and wings during the flare. The analysis of the line profiles from the flare ribbons reveals that the Na I D1 line has a central reversal with excess emission in the blue wing (blue asymmetry). Comparing their observations to radiative simulations, Kuridze et al. (2016) found that the asymmetries of the Na I D1 flare profile are produced by the velocity gradients in the lower solar atmosphere.

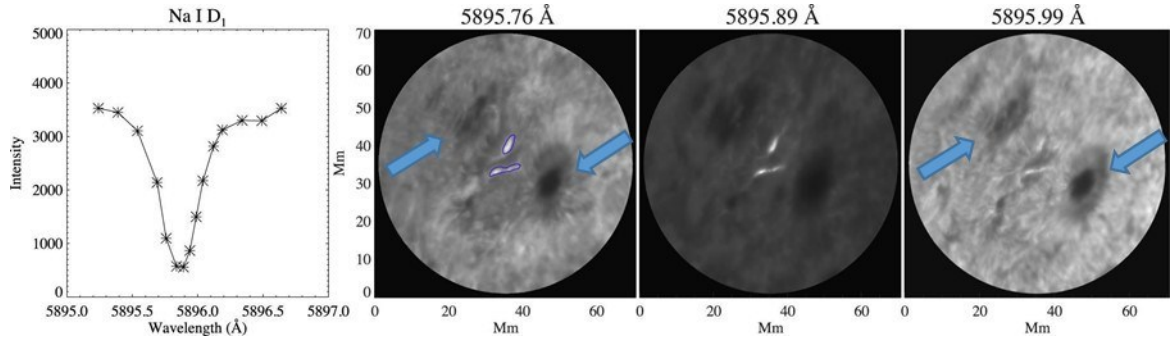

Figure 6: (Adapted from Kuridze et al. 2016). Left: IBIS Na I D1 line profile of a quiet solar region. Asterisks show the spectral positions selected for the IBIS line scan. The full black line shows the mean spectrum averaged over the field of view (FOV) of the quiet Sun. Right: Na I D1 wing and core images at selected wavelength positions. The blue contours show the upper and lower flare ribbons analyzed in the paper. Contours indicate the 50% level of the intensity maximum. The arrows indicate the main sunspots visible in the wings of the spectral line and forming the bipolar AR.

Furthermore, during flares, electron beams, characterized by particular high energy, after having reached the chromosphere in turns, owing to its radiative heating, stimulate the photospheric emission, producing the so-called white light flares (WLFs; Svestka 1966). The involved physical mechanism for the energy transport from the upper chromosphere to the photosphere where the WL emission takes place is well known as “back-warming effect” (Machado, Emslie, & Avrett 1989). The duration of the optical continuum emission at photospheric level is found to vary, but usually associated to the impulsive phase of the corresponding flares. Actually, the white light emission seems to be a common feature of all solar flares (see Hudson, Wolfson, & Metcalf 2006), with the more energetic is the flare, the more detectable is the white light contribution. However, the need of a better and deeper understanding of the physics behind the mechanisms leading to the acceleration of particles and, hence, the increase of the emission in the continuum of the solar spectra or in white light images remains a challenging topic and one of the highest priorities for the worldwide solar physics community investigation.

In this regard, the high resolution of IBIS 2.0 and its capability to scan photospheric and chromospheric lines sequentially represent an important opportunity to understand the spatial and temporal correlations between the emission at chromospheric level and the bright knots observed in photosphere.

Therefore, IBIS 2.0 will be used to address also the following main open questions:

- **Is the white-light emission detectable in all flares?**
- **Can the height of the magnetic reconnection in the solar atmosphere influence the amount of emission at photospheric and chromospheric level?**
- **What is the photospheric magnetic field configuration before, during and after a flare?**
- **What are the polarimetric properties of flare ribbons?**

To this purpose, we will take advantage of IBIS 2.0 measurements to study:

1) the emission in the continuum and its timing with respect to the onset of the flare;
2) the radiative response of the chromosphere and of the photosphere, if any;
3) the photospheric and chromospheric configuration of the magnetic field, also needed as boundary condition for the extrapolations;
4) the plasma motions related to reconfiguration, owing to shear and twist, via Doppler measurements and horizontal tracking;
5) the polarization signal in the flare ribbons.

In the following Table 10, we suggest a possible observing mode for flares.

	FOV and minimum spatial resolution	**S/N ratio**	**Wavelength**	**Observing mode (N° of spectral points, step for each spectral line)**	**Purpose**	**Minimum cadence and duration of observing run**
Phot.	120″ x 120″ @0.16″	1000	Broad-Band	1 image for each spectral point	Detection of WL emission in small flares Location of the WL emission Timing of emission Variations of magnetic field configuration Polarimetric properties around flare ribbons	120 s 6 hours
			Red continuum 668.4	1 pt		
			Fe I 630.2	20 pt, step 5 pm, pol (630.15 & 630.25) 15 pt, step 4 pm, pol (630.15 only)		
Chrom.	120″ x 120″ @0.2″	500	Hα 656.28	15 pt, step 6 pm, no pol	Location of the chromospheric ribbons Timing of emission of the ribbons	
			Ca II 854.2	15 pt, step 4 pm, pol		

Table 10: Flare observations.

3.8 Wave propagation from the photosphere to the upper layers of the solar atmosphere

A plethora of wave signatures, mostly acoustic, have been observed for different magnetic structures (sunspots and small-scale concentrations) at various atmospheric heights, ranging from the deepest photospheric layers through to the outermost corona.

For a long time, wave studies have been performed using a single layer of the solar atmosphere. In the present, multi-instrument multi-layer data are combined to study the wave propagation from the photosphere to the upper atmospheric layers (De Pontieu et al. 2005). It is fundamental to study how the waves propagate, evolve, interact, transform and dissipate during their passage through

the solar atmospheric layers. Many aspects have yet to be determined due to rare observations that trace the wave propagation. When attempting to constrain the energy transfer mechanism, the chromosphere represents an important layer. It is the interface region between the cool photosphere and the hotter corona, where different, rapidly evolving structures with a wide spatial range, high-frequency oscillatory phenomena and magnetically guided compressible and incompressible waves are observed (McIntosh et al. 2011).

Energy propagation is related to magnetic field strength and topology. The p- and f-mode oscillations, interacting with the magnetic field concentrations, can be absorbed and converted into magneto-acoustic waves. These can propagate following the field lines to the upper atmospheric layers (Jess et al. 2017, Pinter & Erdelyi 2018). However, how the p-modes energy would propagate efficiently up is still an open question. This occurs because the waves on their way up encounter a set of obstacles, such as cut-off layers, wave speed gradients, transition region, multi-component plasma, etc. (De Pontieu et al. 2005; McIntosh & Jefferies 2006; Centeno et al. 2009). Another potential observed source that connects all the atmospheric layers and transport energy in the upper atmosphere are vortex motions (or magnetic tornadoes, Wedemeyer-Böhm et al. 2012; Liu et al. 2019).

Usually wave signatures are reported by means of intensity or Doppler velocity measurements (Jess et al. 2017). In addition to these, magnetic field perturbations are also expected. Making use of spectropolarimetric observations, Kupke et al. (2000) suggested that magnetic field fluctuations resulting from oscillations in the Stokes parameters of sunspots could be indicative of field line fluctuations as a response of p-modes. For instance, using a numerical simulation Vigeesh et al. (2011) try to learn how the Stokes-V asymmetries could be a diagnostic tool to study the wave propagation within magnetic flux concentrations. In the same way, sausage and kink modes could be the cause for magnetic oscillations in pores and magnetic concentrations (Fujimura & Tsuneta 2009). Cross-talk with other physical quantities can affect the magnetic oscillation. The phase lag analysis is used to identify intrinsic magnetic fluctuations from cross-talks but its use is restricted to a single photospheric height. **The spectropolarimetric analysis of different solar atmospheric heights allows the application of different diagnostics for the study of magnetic perturbations to be carried out, as already pioneered by Stangalini et al. (2018)** (see Figure 7).

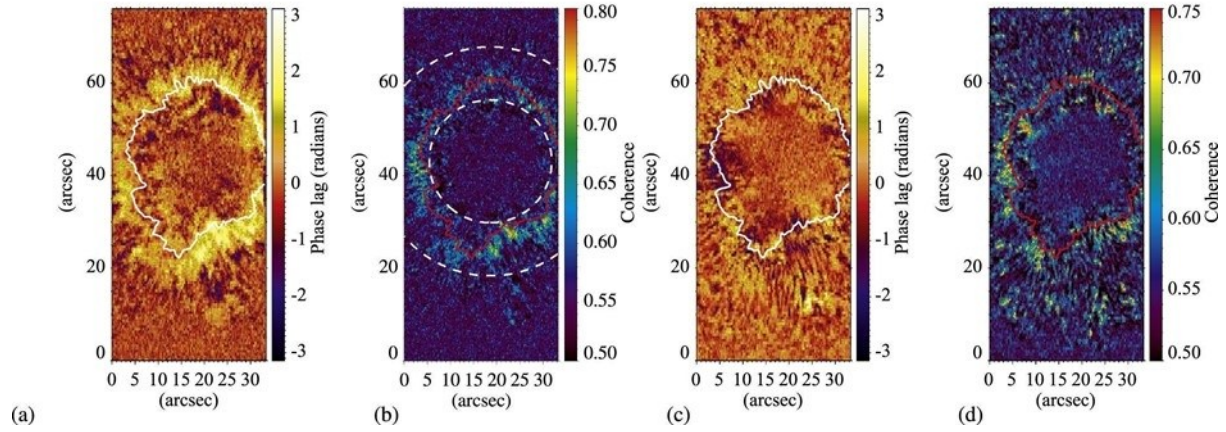

Figure 7: (Adapted from Stangalini et al. 2018). Analysis of the circular polarization (CP) measurements acquired by IBIS in the core of the photospheric Fe I 617.3 nm line and of the chromospheric Ca II 854.2 nm line on 2016 May 20 in the preceding sunspot of active region NOAA 12456. (a) Phase lag map of CP fluctuations at 3 mHz (with a bandwidth of 0.7 mHz) between the photosphere and chromosphere. (b) Coherence map at 3 mHz (with a bandwidth of 0.7 mHz) for the same CP disturbances. (c) Phase lag map at the same frequency band computed between CP fluctuations and core intensity fluctuations in the photosphere. (d) Coherence map corresponding to the phase map of panel (c). The continuous contours indicate the approximate position of the umbra–penumbra boundary as seen in the continuum intensity. The dashed lines highlight the region where the analysis was performed. Note that the maps are obtained by averaging four spectral bins in Fourier space or, equivalently, 3.0 ± 0.7 mHz. For this reason, the average phase and coherence values might appear lower than they are at each frequency bin.

The advent of high-order adaptive optics, high-frequency imaging detectors and the significantly improved data reduction and analysis tools have allowed to probe MHD wave phenomena anywhere close to the intrinsic spatial and temporal scales on which they are believed to operate.

In this context, we hope that IBIS 2.0 with its expected sensitivity may provide spectro-polarimetric measurements of magnetic concentrations at different heights to detect MHD oscillations and track the dynamic evolution as a function of spatial position, time and atmospheric height. This will enable us to address the following open questions:

- **How acoustic and MHD waves are coupled between the different solar atmospheric layers?**
- **How does the magnetic field geometry influence the various MHD wave modes in the different magnetic concentrations?**
- **How does energy transport through the atmosphere occur in magnetic tornadoes?**

In particular, observations acquired with IBIS2.0 will help to analyze:

1) coherence polarization signal using Stokes parameters as diagnostic tools;
2) magnetic field perturbations from the photosphere to the chromosphere via difference of coherence signals;
3) Doppler measurements at different heights.

In the following Table 11, we suggest a possible observing mode for wave studies.

	FOV and minimum spatial resolution	S/N ratio	Wavelength	Observing mode (N° of spectral points, step for each spectral line)	Purpose	Minimum cadence and duration of observing run
Phot.	40″ x 80″ @0.16″	2000	Broad-Band	1 image for each spectral point	Velocity & magnetic field oscillation diagnostics	120 s 4 hours
			Fe I 630.2	20 pt, step 5 pm, pol, (630.15 & 630.25) at fastest cadence possible 15 pt, step 4 pm, pol (630.15 only), at fastest cadence possible		
Chrom.	40″ x 80″ @0.16″	1000	Ca II 854.2	20 pt, step 4 pm, pol, at fastest cadence possible	Magnetic detection of vortices Vortices detection	
			Hα 656.28	15 pt, step 6 pm, no pol		

Table 11: Wave phenomena.

4 Synergies with Present and Next Generation Spectrometers

IBIS 2.0 will play an important role in the study of the coupling between plasma and magnetic field in the lower layers of the solar atmosphere, in coordination with other instruments placed at the focal plane of the present and incoming high resolution telescopes: VTT (Schroter et al. 1985), THEMIS (Mein & Rayrole 1985), SST (Scharmer et al. 2003), GST (Cao et al. 2010), GREGOR (Schmidt et al. 2012), DKIST (Tritschler et al. 2016), SUNRISE3 (Barthol et al. 2018). Indeed, taking into account its science and technical requirements, IBIS2.0 will be complementary to many other instruments for the observations of the Sun from both the Earth and space. Coordinated observing campaigns will benefit from this complementarity on the base of the spectral range, polarimetric sensitivity, field of view, spatial and temporal resolution of IBIS2.0 and the other instruments.

A list of the present and incoming instruments at the main ground-based telescopes are reported in Table 12. Among these important instruments we can mention: LARS@VTT, TESOS@VTT, MTR@THEMIS, GFPI@GREGOR, GRIS@GREGOR, CRISP@SST, CHROMIS@SST, HeSP@SST, VIS@GST, NIRIS@GST, VISP@DKIST, VTF@DKIST, NIRSP@DKIST and CrioNIRSP@DKIST. We also can consider as an important tool for the investigation of the lower layers of the solar atmosphere at high spatial resolution the suite of instruments onboard of the balloon mission SUNRISE3.

Concerning the instruments in the visible range, we emphasize the synergies of IBIS 2.0 with the spectrographs. In fact, a bidimensional spectrometer as IBIS 2.0 allows getting data with a higher spatial and temporal resolution in comparison to a spectrograph, although the other instrument may have higher spectral resolution. For this reason, data taken by spectrographs will be able to integrate IBIS 2.0 data in order to perform a detailed plasma diagnostic.

In particular, considering IBIS 2.0 at the VTT focal plane, it will also be possible to obtain simultaneous observations with a spectrograph situated at a different floor at the same telescope, working in the visible range as well. This could represent a great opportunity, as we will be observing cospatial regions of the Sun using two instruments with the same telescope, even if with different methods of measurement. Moreover, the simultaneous use of a spectrograph at VTT will enhance the precision of the absolute velocity calibration for IBIS 2.0, when encompassing the same spectral lines used in the IBIS 2.0 observations. Also, they will make possible simultaneous observations of the photosphere and chromosphere, although with two different instruments.

IBIS 2.0 is also expected to benefit from a hopefully high spectropolarimetric sensitivity. Indeed, in IBIS, it was estimated by in Viticchié et al. (2010) as 10^{-3} times the continuum intensity level. This peculiar strength will enable a fruitful collaboration with other instruments mounted in Canary Islands at telescopes with better spatial resolution but a slightly lower polarimetric sensitivity. For instance, this is about 5×10^{-3} in CRISP@SST (e.g., Díaz Baso et al. 2019).

VTF will be one among the first-light instruments of DKIST, the first 4-m aperture solar telescope in the world. This instrument is designed as a diffraction-limited narrowband tunable instrument for Stokes spectropolarimetry in the wavelength range between 520 and 860 nm, i.e., in an overlapping spectral range to IBIS 2.0. The VTF@DKIST will have a field of view of one arc minute squared, with a pixel scale of 0.014″ on the sky and a spectral resolution of 6 pm at a wavelength of 600 nm. Therefore, VTF@DKIST will provide data with really higher performances in comparison with other bidimensional spectrometers.

However, it is important to highlight that IBIS 2.0 at VTT focal plane, together with the other spectrometers in Canary Islands, will cover a different time window, providing the possibility to study the evolution of many phenomena with good temporal continuity, although with a different FOV and lower spatial resolution. Note that, at the time of writing, the NIRSP, CrioNIRSP, and VTF instruments are still under development.

TELESCOPE	VIS	NIR	NUV
GREGOR	**GFPI (530-860 nm)** [9]	**GRIS (1000-1800 nm)** [3]	
VTT	LARS (400-700 nm) [8] TESOS (450-750 nm) [6]		
THEMIS	MTR (450-850 nm) [10]		
SST	**CRISP (510-860 nm)** [12] **MiHI (630.2 nm)**	**HeSP (1000-1100 nm)**	CHROMIS (390-490 nm) [11]
GST	**VIS (550-700 nm)** [2]	**NIRIS (1000-1600 nm)** [1]	
DKIST	VISP (380-900 nm) [4] **VTF (520-870 nm)** [13]	NIRSP (500-2500 nm) [5] CrioNIRSP (1000-5000 nm) [7]	
SUNRISE III	**TuMaG (520-530 nm)**	SCIP (765-855 nm)	SUSI (300-430nm)

Table 12: Present and incoming spectrometers at ground-based telescopes. Black boldface indicates the spectropolarimeters based on Fabry-Pérot devices, black color the spectrometers based on Fabry-Pérot, red color the linear spectropolarimeters, red boldface the integral field unit instruments. The superscript numbers indicate the corresponding references listed for Section 4, reported in Section 6.

A similar coordination can be performed between IBIS 2.0 and VIS, the spectrometer mounted at the GST (aperture 1.6 m), which operates at Big Bear Observatory, in California.

Among the other instruments, there is an obvious complementarity due to the different spectral ranges covered by some of them. Indeed, the combination of observations of the photosphere and chromosphere in the visible range with observations in Near Infrared (NIR) and Near Ultraviolet (NUV) has a great potentiality for investigating the above-mentioned scientific cases. In this regard, a separate document will describe the advantages and the scientific interests of observations performed in the NIR and NUV with a future, upgraded version of IBIS 2.0 (see [RD3]).

Further synergies in the study of the chromosphere can be represented by joint observations with the Atacama Large Millimeter Array (ALMA; Wootten & Thompson 2009) in the millimeter wavelength range. In this radio frequency, continuum radiation originates from free–free emission in the chromosphere and the brightness temperature can provide an observable directly related to the electron temperature of the chromospheric plasma. In this context, strong correlations have been recently observed between the brightness temperature observed in ALMA Band 3 (3 mm; 100 GHz) and the core width of the Hα 656.3 nm line observed with IBIS (Molnar et al. 2019). However, it must be mentioned that with IBIS 2.0 at the VTT focal plane, there will be a difference of four time zones between ALMA and IBIS 2.0. Furthermore, simultaneous observations with other radio facilities led by INAF, such as the Medicina antenna (32 m) and the Sardinia Radio

Telescope (64 m) in K-band (18-26 GHz), with future high-frequency/high-resolution solar imaging up to 100 GHz in full-Stokes polarimetric mode, will be fundamental to complement their measurements of the brightness temperature of the radio quiet-Sun component and the study of the long-term evolution of active features.

In addition to the aforementioned synergy with ground-based facilities, we highlight the possibility of using IBIS 2.0 in coordination with space telescopes, such as the instruments on board the Hinode, IRIS, and Solar Orbiter missions. Indeed, coordinated campaigns between IBIS and satellite telescopes were already successfully carried out in the past years. The optical telescope aboard Hinode (SOT, Tsuneta et al. 2008) is currently only partially working, but regularly taking data using the spectropolarimeter (SP), which acquires photospheric Stokes profiles along the Fe I 630.2 nm line pair, benefitting from a high spectral resolution ($R \approx 200000$) and a polarimetric sensitivity down to $5x10^{-4}$. These data may complement those acquired by IBIS 2.0 in several cases. Besides, IRIS (Interface Region Imaging Spectrograph, De Pontieu et al. 2014) operates in spectroscopic and imaging modes in the UV (133 - 283 nm) with a focus on the dynamics of the transition region. The information provided by IBIS 2.0 relevant to the chromospheric level fits well in a scenario of multi-layers studies of transition region phenomena, for which the chromosphere is the lower boundary.

In this perspective, coordination with future observations carried out by the remote sensing instruments aboard Solar Orbiter (Müller et al. 2013) that will begin in late 2021, is highly desirable. For instance, photospheric measurements acquired by SolO/PHI will need synergistic observations from a different point of view to fully exploit their potential. The coupling between the low atmospheric layers, in particular the chromosphere, and the outer corona, which will be observed by SolO/Metis, will also benefit from IBIS2.0 capabilities to characterize the properties of the regions of pumping radiation as well as of the sites of solar wind acceleration.

In this context, IBIS2.0 will also contribute in monitoring the heliospheric conditions in which the Parker Solar Probe (Fox et al. 2016) in-situ mission is operating, as well as the environment where upcoming interplanetary missions, such as BepiColombo and Juice, will move. Moreover, IBIS2.0 will provide information about the Space Weather conditions, adding its valuable contribution to those of many other facilities currently operating.

5 Summary

IBIS 2.0 is a new version of a previous instrument (IBIS; Cavallini et al. 2001, 2006) which was built by the INAF-Arcetri Astrophysical Observatory, in collaboration by the Dept. of Physics and Astronomy of the University of Florence, and the Dept. of Physics of the University of Rome "Tor Vergata". IBIS was a double Fabry-Perot system working in the 580-860 nm range. First installed in mid 2003 at the 76 cm Dunn Solar Telescope (DST) of the US National Solar Observatory (NSO), it has since been upgraded to a full Stokes-polarimeter with important contributions from both the NSO and the US High Altitude Observatory (HAO). Throughout the years, IBIS has produced a variety of scientific results spanning from the photospheric dynamics at super granular scales to the evolution of fine photospheric and chromospheric magnetic structures. A list of relevant published papers (about 100) is given in Appendix B of [RD2].

This upgraded version will work in the same spectral range as the previous one and will be a pathfinder for several scientific topics that have been described in the present document. IBIS 2.0 will contribute to the study of many debated aspects of the physical phenomena occurring the solar atmosphere by **sampling in rapid succession several spectral lines formed at different heights**. In fact, this is a crucial capability as it allows investigations on the propagation of perturbations throughout the solar atmosphere, or on the variation with height of the magnetic field configuration. On the base of the available narrowband prefilters, IBIS 2.0 Fabry-Perot interferometers will be rapidly tuned, to allow sequential scanning along the spectral lines of interest, which are reported in Table 1.

In this regard, IBIS 2.0 is expected to provide an important contribution to the study of many scientific topics for Solar Physics and to answer to many open questions related to the knowledge of plasma and its magnetic properties at different heights in the solar atmosphere.

- Are there chromospheric counterparts of *umbral dots*?
- Are *umbral dots* heated due to oscillatory magnetoconvection, penetration of hot plasma between thin flux tubes or electric currents?
- Are *moving magnetic features* extensions of penumbral filaments?
- Which is the source of *plasma jets in sunspot light bridges*?
- Is the overlying magnetic canopy responsible for both the *penumbra formation and decay* processes?

IBIS 2.0 is expected to be characterized by a **highly stable imaging spectropolarimetry** with repeatable performances. This aspect will be very useful to:

- perform a patrol of the *quiet Sun* using daily data taken at the solar disc center, also useful for solar irradiance measurements;
- probe *MHD waves* phenomena as a function of spatial position, time and atmospheric height in and around the main features of the solar atmosphere;
- describe the spectropolarimetric signatures observed in the Stokes profiles during *magnetic flux cancellation* in the low solar atmosphere;
- derive some signatures of the rising plasma in *emerging flux regions*, e.g., time delays during the passage through different atmospheric heights and vertical velocities

IBIS 2.0 is expected to show its **best performances in the study of chromospheric dynamics**. In particular, through the CaII triplet (849.8; 854.2; 866.2 nm) spectral range, it will provide a unique contribution to the interpretation of many chromospheric phenomena, such as magnetic reconnection, plasma acceleration, flare secondary effects, etc:

- Which is the response of the solar chromosphere to the energy release due to the *interaction between pre-existing and emerging magnetic flux*?
- Can the height of the magnetic reconnection during a *flare* influence the amount of emission at photospheric and chromospheric level?
- What are the *polarimetric properties of flare ribbons*?

IBIS 2.0 is planned to be employed in coordinated observing campaign with ground-based and space telescopes in order to exploit the complementary characteristics of this instrument with other present and incoming instruments dedicated to the study of the Sun. IBIS 2.0 will take advantage from synergies with other ground-based instruments:

- observing in other energy bands (NIR and NUV),
- covering other time windows,
- using other measurement methods (spectrographs),
- exploiting different polarimetric sensitivity

Taking into account the scientific goals which can be achieved by IBIS 2.0, we indicated some **requirements** reported in the Tables that are supplied in Section 3 of the present document. In particular, we highlight the importance to obtain the best performances in terms of speed and stability to sample different spectral lines with different observation modes.

It is worth noting that these requirements are necessary the primary goals of the aforementioned science cases. However, even if IBIS2.0 could not completely achieve those requirements, we think that significant progresses may be obtained, provided that appropriate trade-offs are taken into account.

The main technical constraint that is able to satisfy the scientific requirements is its wide flexibility in the spectral sampling, i.e., using a different number of points along each line and different steps. Two main observation modes are required for each wavelength scan: a scan of the spectral lines taking 1 image for each spectral point sequentially or taking several images at the same spectral points for each step. Moreover, it is also necessary to guarantee the possibility to sample more than one spectral line during an observing run, both sequentially and repeating the scan of each line several times before to scan a subsequent one. Finally, we expect that a user-friendly approach to IBIS 2.0, which includes both high flexibility in data acquisition and automatized data reduction, will provide a strong appeal for potential observers.

Finally, we think that an important future project may be a new bidimensional spectrometer that is **able to operate in NIR or NUV energy bands**. In fact, we think that another instrument with the same performances of IBIS 2.0, which is suitable to observe in those energy bands, could be an appetible instrument for the new generation telescopes, such as the European Solar Telescope (EST; Collados et al. 2010). Moreover, it could represent an important opportunity for the Italian solar community to develop a competitive instrument in the context of the best ground-based telescopes for Solar Physics in the world.

6 Bibliography

Section 1

[1]Berlicki, A., Mein, P., & Schmieder, B. 2006, A&A, 445, 1127

[2]Cauzzi, G., Reardon, K. P., Uitenbroek, H., et al. 2008, A&A, 480, 515

[3]Del Moro, D., Giordano, S. & Berrilli, F. 2007, A&A, 472, 599

[4]Eibe, M. T., Mein, P., Roudier, T., & Faurobert, M. 2001, A&A, 371, 1128

[5]Finsterle, W., Jefferies, S. M., Cacciani, A., et al. 2004, ESA-SP, 223

[6]Kucera, A., Balthasar, H., Rybak, J., et al. 1998, A&A, 332, 1069

[7]Norton, A. A., Graham, J. P., Ulrich, R. K., et al. 2006, Sol. Phys., 239, 69

[8]Penn, M. J., & Jones, H. P. 1996, Sol. Phys., 168, 19

[9]Tomita, Y. 1960, PASJ, 12, 524

[10]Uitenbroek, H. 2004, ESA-SP, 107

[11]Vernazza, J. E., Avrett, E. H., & Loeser, R. 1981, ApJ Supp. Ser., 45, 635

Section 3.2

Abramenko, V. I. 2017, MNRAS, 471, 3871

Abramenko, V. I. 2018, MNRAS, 480, 1607

Bellot Rubio, L. R., Ruiz Cobo, B., & Collados, M. 2000, ApJ, 535, 489

Berrilli, F., Del Moro, D., Russo, S., et al. 2005, ApJ, 632, 677

Danilovic, S., Schüssler, M., & Solanki, S. K. 2010, A&A, 509, A76

Del Moro, D., Giannattasio, F., Berrilli, F., et al. 2015, A&A, 576, A47

Giannattasio, F., Del Moro, D., Berrilli, F., et al. 2013, ApJL, 770, L36

Giannattasio, F., Stangalini, M., Berrilli, F., et al. 2014a, ApJ, 788, 137

Giannattasio, F., Berrilli, F., Biferale, L., et al. 2014b, A&A, 569, A121

Giannattasio, F., Berrilli, F., Consolini, G., et al. 2018, A&A, 611, A56

Hanasoge, S. M., Duvall, T. L., Sreenivasan, K. R. 2012, Proceedings of the National Academy of Science, 109, 11928

Parker, E. N. 1978, ApJ, 221, 368

Petrovay, K., & Szakaly, G. 1993, A&A, 274, 543

Spruit, H.C. 1979, Sol. Phys., 61, 363

Utz, D., Jurčák, J., Hanslmeier, A., et al. 2013, A&A, 554, A65

Viticchié, B., Del Moro, D., Berrilli, F., et al. 2009, ApJL, 700, L145

Viticchié, B., Del Moro, D., Criscuoli, S., et al. 2010, ApJ, 723, 787

Section 3.3

Asai, A., Ishii, T.T., Kurokawa, H. 2001, ApJ, 555, L65

Bharti, L., Beeck, B., & Schüssler, M. 2010, A&A, 510, A12
Criscuoli, S., Del Moro, D., Giannattasio, F., et al. 2012, A&A, 546, A26
Hagenaar, H. J., & Shine, R. A. 2005, ApJ, 635, 659
Harvey, K. L., & Harvey, J. 1973, Sol. Phys., 28, 61
Lites, B. W., Scharmer, G. B., Berger, T. E., & Title, A. M. 2004, Sol. Phys., 221, 65
Louis, R. E., Bellot Rubio, L. R., Mathew, S. K., & Venkatakrishnan, P. 2009, ApJ, 704, L29
Louis, R. E., Mathew, S. K., Bellot Rubio, L. R., et al. 2012, ApJ, 752, 109
Rempel, M. 2012, ApJ, 750, 62R
Rimmele, T. R. 1997, ApJ, 490, 458
Rimmele, T. 2008, ApJ, 672, 684
Sainz Dalda, A., & Bellot Rubio, L. R. 2008, A&A, 481, L21
Schlichenmaier, R. 2002, Astron. Nach., 323, 303
Shimizu, T., Katsukawa, Y., Kubo, M., et al. 2009, ApJ, 696, L66
Shine, T., & Title, A. 2001, in Encyclopedia of A&A, ed. P. Murdin, 4, 3209
Solanki, S. K. 2003, A&AR, 11, 153
Spruit, H.C., Scharmer, G. B. 2006, A&A, 447, 343
Verma, M., Balthasar, H., Deng, N., et al. 2012, A&A, 538, A109
Zuccarello, F., Romano, P., Guglielmino, S. L., et al. 2009, A&A, 500, L5

Section 3.4

Bharti, L., Hirzberger, J., & Solanki, S. K. 2013, A&A, 552, L1
Benko, M., Gonzalez, M. Balthasar, H. et al. 2018, A&A, 620, A191
Jurčák, J. 2011, A&A, 531, A118
Jurčák, J., Bello González, N., et al. 2015, A&A, 580, L1
Katsukawa, Y., Berger, T. E., Ichimoto, K., et al. 2007, Science, 318, 1594
Leka, K. D., & Skumanich, A. 1988, ApJ, 507, 454
Murabito, M., Romano, Guglielmino, S. L., et al. 2016, ApJ, 825, 75
Murabito, M., Zuccarello, F., Guglielmino, S. L. et al., 2018, ApJ, 855, 58
Murabito, M., Ermolli, I., Giorgi, F., et al. 2019, ApJ, 873, 126
Murabito, M., Guglielmino, S. L., Ermolli, I., et al. 2020, ApJ, 890, 96
Romano, P., Frasca, D., Guglielmino, S. L., et al. 2013, ApJ, 771, L3
Romano, P., Guglielmino, S. L., Cristaldi, A., et al. 2014, ApJ, 784, 10
Shimizu, T., Ichimoto, K, & Suematsu, Y., 2012, ApJL, 747, L18
Tiwari, S. K., van Noort, M., Lagg, A., et al. 2013, A&A, 557, A25
Tiwari, S. K., Moore, R. L., Winebarger, A. R., & Alpert, S. E. 2016, ApJ, 816, 92
Verma, M., Denker, C., Balthasar, H., et al. 2018, A&A, 614, 2
Watanabe, H., Kitai, R., & Otsuji, K. 2014, ApJ, 796, 77
Zuccarello, F., Guglielmino, S. L., Capparelli, V., et al. 2020, ApJ, 889, 65

Section 3.5

Bellot Rubio, L. R., & Beck, C. 2005, ApJL, 626, L125

Chae, J., Moon, Y.-J., & Pevtsov, A. A. 2004, ApJL, 602, L65

Deng, N., Chen, X., Liu, C., et al. 2015, ApJ, 799, 219

Kaithakkal, A. J., & Solanki, S. K. 2019, A&A, 622, A200

Kaithakkal, A. J., Borrero, J. M., Fischer, C. E., et al. 2020, A&A, 634, A131

Kubo, M., Chye Low, B., & Lites, B. W. 2014, ApJL, 793, L9

Harvey, K. L., Jones, H. P., Schrijver, C. J., et al. 1999, Sol. Phys., 190, 35

Litvinenko, Y. E. 1999, ApJ, 515, 435

Livi, S. H. B., Martin, S. F., Wang, H., & Ai, G. 1989, Sol. Phys., 121, 197

Panesar, N. K., Sterling, A. C., Moore, R. L., & Chakrapani, P. 2016, ApJL, 832, L7

van Ballegooijen, A. A. & Martens, P. C. H. 1989, ApJ, 343, 971

Section 3.6

Archontis, V., Moreno-Insertis, F., Galsgaard, K., et al. 2004, A&A, 426, 1047

Archontis, V., Hood, A. W., & Brady, C. 2007, A&A, 466, 367

Archontis, V., & Hood, A. W. 2009, A&A, 508, 1469

Cheung, M. C. M., & Isobe, H. 2014, Living Reviews in Solar Physics, 11, 3

Centeno, R., Blanco Rodríguez, J., Del Toro Iniesta, J. C., et al. 2017, ApJ Supp. Ser., 229, 3

Ellerman, F. 1917, ApJ, 46, 298

Galsgaard, K., Archontis, V., Moreno-Insertis, F., et al. 2007, ApJ, 666, 516

Guglielmino, S. L., Zuccarello, F., Romano, P., & Bellot Rubio, L. R. 2008, ApJL, 688, L111

Guglielmino, S. L., Bellot Rubio, L. R., Zuccarello, F., et al. 2010, ApJ, 724, 1083

Guglielmino, S. L. 2012, 4th Hinode Science Meeting: Unsolved Problems and Recent Insights, 109

Guglielmino, S. L., Zuccarello, F., Young, P. R., et al. 2018, ApJ, 856, 127

Guglielmino, S. L., Young, P.~R., & Zuccarello, F. 2019, ApJ, 871, 82

Hansteen, V. H., Archontis, V., Pereira, T. M. D., et al. 2017, ApJ, 839, 22

Nelson, C. J., Shelyag, S., Mathioudakis, M., et al. 2013, ApJ, 779, 125

Ortiz, A., Bellot Rubio, L. R., Hansteen, V. H., et al. 2014, ApJ, 781, 126

Ortiz, A., Hansteen, V. H., Bellot Rubio, L. R., et al. 2016, ApJ, 825, 93

Toriumi, S., Katsukawa, Y., & Cheung, M. C. M. 2017, ApJ, 836, 63

Vargas Domínguez, S., van Driel-Gesztelyi, L., & Bellot Rubio, L. R. 2012, Sol. Phys., 278, 99

Vissers, G. J. M., Rouppe van der Voort, L. H. M., Rutten, R. J., et al. 2015, ApJ, 812, 11

Vissers, G. J. M., de la Cruz Rodríguez, J., Libbrecht, T., et al. 2019, A&A, 627, A101

Yokoyama, T., & Shibata, K. 1995, Nature, 375, 42

Young, P. R., Tian, H., Peter, H., et al. 2018, Space Sci. Rev., 214, 120

Section 3.7

Carmichael, H. 1964, Proc. AAS-NASA Symp. – The Physics of Solar Flares, ed. W. N. Hess (Washington: NASA, Science and Technical Information Division), 451

Fletcher, L., & Hudson, H. S. 2008, ApJ, 675, 1645

Harrison, R. A. 1986, A&A, 162, 283

Hirayama, T. 1974, Sol. Phys., 34, 323

Hudson, H. S., Wolfson, C. J., & Metcalf, T. R. 2006, Sol. Phys., 234, 79

Kopp, R. A. & Pneuman, G. W. 1976, Sol. Phys., 50, 85

Kuridze, D., Mathioudakis, M., Christian, D. J., et al. 2016, ApJ, 832, 147

Machado, M. E., Emslie, A. G., & Avrett, E. H. 1989, Sol. Phys., 124, 303

Matthews, S. A., van Driel-Gesztelyi, L., Hudson, H. S., & Nitta, N. V. 2003, A&A, 409, 1107

Metcalf, T. R., Alexander, D., Hudson, H. S., & Longcope, D. W. 2003, ApJ, 595, 483

Priest, E. R., & Forbes, T. G. 2000, Magnetic Reconnection (Cambridge University Press)

Priest, E. R., & Forbes, T. G. 2002, A&ARv, 10, 313

Sui, L., Holman, G. D., & Dennis, B. R. 2005, ApJ, 626, 1102

Sturrock, P. A. 1966, Nature, 211, 695

Švestka, Z. 1966, Space Sci. Rev., 5, 388

Section 3.8

Centeno, R., Collados, M., & Trujillo Bueno, J. 2009, ApJ, 692, 1211

De Pontieu, B., Erdélyi, R., & De Moortel, I. 2005, ApJL, 624, L61

Fujimura, D. & Tsuneta, S. 2009, ApJ, 702, 1443

Jess, D. B., Van Doorsselaere, T., Verth, G., et al. 2017, ApJ, 842, 59

Kupke, R., Labonte, B. J., & Mickey, D. L. 2000, Sol. Phys., 191, 97

Liu, J., Nelson, C. J., & Erdélyi, R. 2019, ApJ, 872, 22

McIntosh, S. W. & Jefferies, S. M. 2006, ApJL, 647, L77

McIntosh, S. W., De Pontieu B., Carlsson M., et al. 2011, Nature, 475, 477

Pintér, B., & Erdélyi, R. 2018, Advances in Space Research, 61, 759

Stangalini, M., Jafarzadeh, S., Ermolli, I., et al. 2018, ApJ, 869, 110

Vigeesh, G., Steiner, O., & Hasan, S. S. 2011, Sol. Phys., 273, 15

Wedemeyer-Böhm, S., Scullion, E., Steiner, O., et al. 2012, Nature, 486, 505

Section 4

Barthol, P., Katsukawa, Y., Lagg, A., et al. 2018, 42nd COSPAR Scientific Assembly, PSB.1-28-1

[1]Cao W., Goode P., Ahn P., Gorceix N., et al., 2012, ASP Conf. Ser., 463, 291

[2]Cao, W., Gorceix, N., Coulter, R., et al. 2010, Astron. Nach., 331, 636

[3]Collados, M., López, R., Páez, E., et al. 2012, Astron. Nach., 333, 872

[4]de Wijn, A. G., Casini, R., Nelson, P. G., et al. 2012, in Proc. SPIE, 84466X

Díaz Baso, C. J., Martínez González, M. J., Asensio Ramos, A., et al. 2019, A&A, 623, A178

De Pontieu, B., Title, A. M., Lemen, J. R., et al. 2014, Sol. Phys., 289, 2733

Fox, N. J., Velli, M. C., Bale, S. D., et al. 2016, Space Science Reviews, 204, 7

[5]Jaeggli, S. A., Anan, T., Kramar, M., et al. 2019, AAS Meeting Abstracts 234, 106.12

[6]Kentischer, T. J., Schmidt, W., Sigwarth, M., et al. 1998, A&A, 340, 569

[7]Kuhn, J. R., Scholl, I. F., & Mickey, D. L. 2012, Second ATST-EAST Meeting: Magnetic Fields from the Photosphere to the Corona, 207

[8]Löhner-Böttcher, J., Schmidt, W., Doerr, H. P., et al. 2017, A&A, 607, A12

Mein, P., & Rayrole, J. 1985, Vistas Astron., 28, 567

Molnar, M. E., Reardon, K. P., Chai, Y., et al. 2019, ApJ, 881, 99

Müller, D., Marsden, R. G., St. Cyr, O. C., et al. 2013, Sol. Phys, 285, 25

[9]Puschmann, K. G., Denker, C., Kneer, F., et al. 2012, Astron. Nach., 333, 880

[10]Rayrole, J., & Mein, P. 1994, IAU Colloquium no. 141, p.170

Rimmele, T. R., Berukoff, S., et al. 2016, Astron. Nach., 337, 1064

[11]Scharmer, G. 2017, in SOLARNET IV: The Physics of the Sun from the Interior to the Outer Atmosphere, 85

Scharmer, G. B., Bjelksjo, K., Korhonen, T. K., et al. 2003, in Proc. SPIE, Vol. 4853, 341–350

[12]Scharmer, G. B., Narayan, G., Hillberg, T., et al. 2008, ApJ, 689, L69

Scharmer, G. B., Löfdahl, M. G., Sliepen, G., et al. 2019, A&A, 626, A55

Schmidt, W., von der Lühe, O., Volkmer, R., et al. 2012, Astron. Nach., 333, 796

[13]Schmidt, W., Bell, A., Halbgewachs, C., et al. 2014, in Proc. SPIE, 9147

Schroter, E. H., Solatu, D., & Wiehr, E. 1985, Vistas Astron., 28, 519

Suematsu, Y., Katsukawa, Y., Hara, H., et al. 2018, 42nd COSPAR Scientific Assembly, PSB.1-29-18

Tsuneta, S., Ichimoto, K., Katsukawa, Y., et al. 2008, Sol. Phys., 249, 167

Wootten, A., & Thompson, A. R. 2009, IEEE Proceedings, 97, 1463

Section 5

Cavallini, F., Berrilli, F., Cantarano, S., et al. 2001, MemSAIt, 72, 554

Cavallini, F. 2006, Sol. Phys., 236, 415

Collados, M., Bettonvil, F., Cavaller, L., & EST Team 2010, Astron. Nach., 331, 615

--- End of document ---